Supporting Information

High-frequency pulsed electron-electron double resonance spectroscopy on DNA duplexes using trityl tags and shaped microwave pulses

A. Kuzhelev,‡[a,b,c] D. Akhmetzyanov,‡[d] V. Denysenkov,[d] G. Shevelev,[a,e] O. Krumkacheva,[a,c] E. Bagryanskaya*[a,b] and T. Prisner*[d]

[a] *Novosibirsk State University, Pirogova 1, 630090 Novosibirsk, Russia.*
[b] *N. N. Vorozhtsov Novosibirsk Institute of Organic Chemistry SB RAS, Lavrentiev Avenue 9, 630090 Novosibirsk, Russia. E-mail: egbagryanskaya@nioch.nsc.ru*
[c] *International Tomography Center SB RAS, Institutskaya 3a, 630090, Novosibirsk, Russia*
[d] *Goethe University Frankfurt am Main, Institute of Physical and Theoretical Chemistry and Center for Biomolecular Magnetic Resonance, Max von Laue Str. 7, 60438 Frankfurt am Main, Germany. E-mail: prisner@chemie.uni-frankfurt.de*
[e] *Institute of Chemical Biology and Fundamental Medicine SB RAS, Lavrentiev Avenue 8, 630090 Novosibirsk, Russia*

‡ *Authors contributed equally to the work.*

* *Corresponding authors.*

Table of Content:

I. Experimental part

The concentration of studied 10-mer and 17-mer DNA duplexes was about $1.5 \cdot 10^{-5}$ M in D_2O: glycerol-d_8, 1:1, v:v, with 10 mM sodium cacodylate. The detailed synthesis of the duplexes and characterization by pulsed EPR spectroscopy at 34 GHz frequencies and MD simulations were published elsewhere.[1]

The concentration of finland trityl was roughly $3 \cdot 10^{-5}$ M in D_2O:glycerol-d_8, 1:1, v:v, with about 110 mM sodium chloride.

180 GHz pulsed EPR measurements

Pulsed EPR measurements at 180 GHz frequencies were performed on a home built G-band EPR spectrometer[2,3] with a microwave power of about 100 mW. The sample temperature was 40 K for all measurements. For the pulse experiments the samples were transferred into quartz tubes (I.D. 0.4 mm, O.D. 0.55 mm). The field-swept Hahn echo-detected EPR spectrum was recorded with pulse lengths of 36 ns and 52 ns. The pulse separation time τ was set to 200 ns. Shot repetition time was 35 ms and the number of shots per point was 10 for all pulse experiments. We used the dead-time free four-pulse PELDOR/DEER sequence.[4,5] The frequency offset between pump and observer pulses was 40 MHz, as indicated in Figure 1. For the 10-mer DNA the detection pulse lengths were 30-34 ns and 48-50 ns, for the $\pi/2$ and π pulses, respectively, and 42-48 ns for the pump pulse. The separation between the first $\pi/2$ and π observer pulses was 250 ns and kept constantly for all PELDOR experiments. The dipolar evolution time window was 8.2 μs. The number of points was 251 and the number of scans 120-200 resulting in a total accumulation time of about 3-5 hours. For 17-mer DNA the detection pulse lengths were 28 ns and 48 ns, for the $\pi/2$ and π pulses, respectively, and 36 ns for the pump pulse. The dipolar evolution time window was set to 9.2 μs. The number of data points was 301 and the number of scans 100-180 resulting in a total accumulation time of about 3-5 hours.

260 GHz pulsed EPR measurements

Pulsed EPR measurements at 260 GHz frequency were performed on a 260 GHz Bruker Elexsys E780 EPR spectrometer. The system is equipped with a 9.4 T superconducting magnet, with a quasi-optical front-end with a microwave power of about 15 mW and an arbitrary waveform generator (AWG). For the experiments the samples were transferred into quartz tubes (I.D. 0.2 mm, O.D. 0.33 mm). The echo-detected EPR spectrum was recorded with pulse lengths of 64/110 ns and 60/100 ns at a temperature of 50 K and 40 K for the 10 nuc-DNA and 17 nuc-DNA, respectively. The pulse separation time τ was 400 ns. Shot repetition time was set to 20 ms and the number of shot per point was 50. 260 GHz PELDOR measurements were performed at 50 K using

the standard four-pulse, dead time-free PELDOR/DEER sequence with a 64-phase cycle.[6] For the 10-mer DNA the π/2 and π detection pulses was 70/110 ns. The pulse separation between the two first observer pulses was fixed to 1 μs for all PELDOR experiments. The dipolar evolution time window was 7 μs, with 148 time steps of 40 ns. The shot repetition time was 12 ms with 5 shots per point averaging and a pump-probe frequency offset (indicated in Figure 1) of 60 MHz for all measurements. For the PELDOR experiments the pump pulse length was 110 and 400 ns for rectangular and adiabatic (sech/tanh) pulses, respectively. The shape and inversion profile of the adiabatic pulse are shown in Figure S4 and S5, respectively (explained in more detail below). The number of scans was 57 corresponding to a total accumulation time of about 9 hours. For the 17-mer DNA the π/2 and π detection pulses were 64/100 ns long. The dipolar evolution time window was 9 μs, with 207 time steps of 40 ns. The number of scans was 39 corresponding to a total accumulation time of about 9 hours.

II. EPR spectra of 10mer DNA and Finland trityl at 180 GHz

An overlay of the EPR spectra of the 10mer DNA and the Finland trityl radical obtained at 180 GHz microwave frequency and a temperature of 40 K are presented in Figure S1. As can be seen the EPR spectra differ only insignificantly. The spectra were obtained with the following pulse parameters: the length of π/2 and π pulses were 36 ns and 50 ns (for Finland trityl the length of π pulse was 64 ns), respectively, with a pulse separation τ of 200 ns, a 35 ms repetition time and 10 shots averaged.

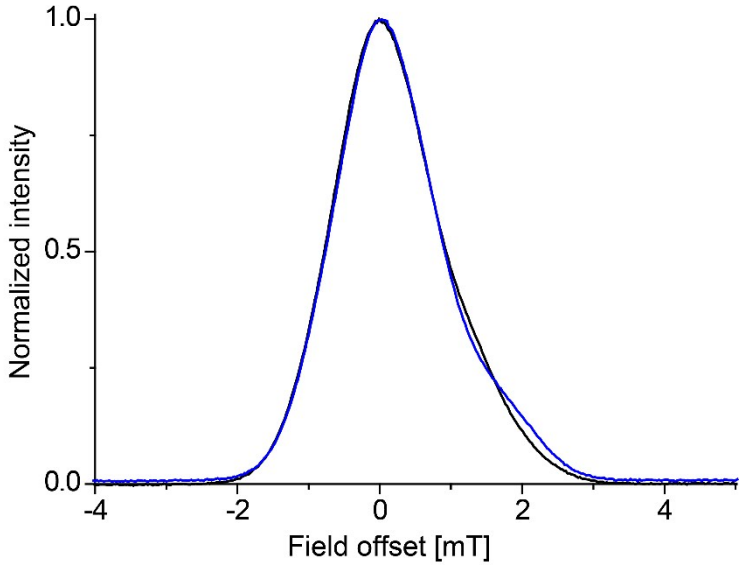

Figure S1. 180 GHz EPR spectra of 10mer DNA (black curve) and Finland trityl (blue curve) obtained at a temperature of 40 K. The axis of the abscissa corresponds to the field offset from the maximum absorption position in the spectrum.

III. Electron spin relaxation

The experimental T_1 and T_2 relaxation measurements of the 10 and 17mer DNAs obtained at 180 and 260 GHz frequencies and of the Finland trityl radical at 180 GHz are depicted in Figure S2. The obtained values of the electron spin relaxation times are listed in Table S1. The electron spin longitudinal relaxation times T_1 were obtained from fitting of the experimental time traces with a mono-exponential function, whereas the reported transversal relaxation times T_m correspond to the time constant after which the Hahn echo signal decayed by a factor of e.

Table S1. Electron spin relaxation times for the 10 and 17mer DNAs at 180 and 260 GHz frequencies

Sample	Frequency / GHz	Temperature / K	T_m / μs	T_1 / ms
Finland trityl	180	40	4.8	13.0
10mer DNA	180	40	4.1	13.0
10mer DNA	260	50	4.0	6.0
17mer DNA	180	40	4.0	11.5
17mer DNA	260	50	4.0	5.5

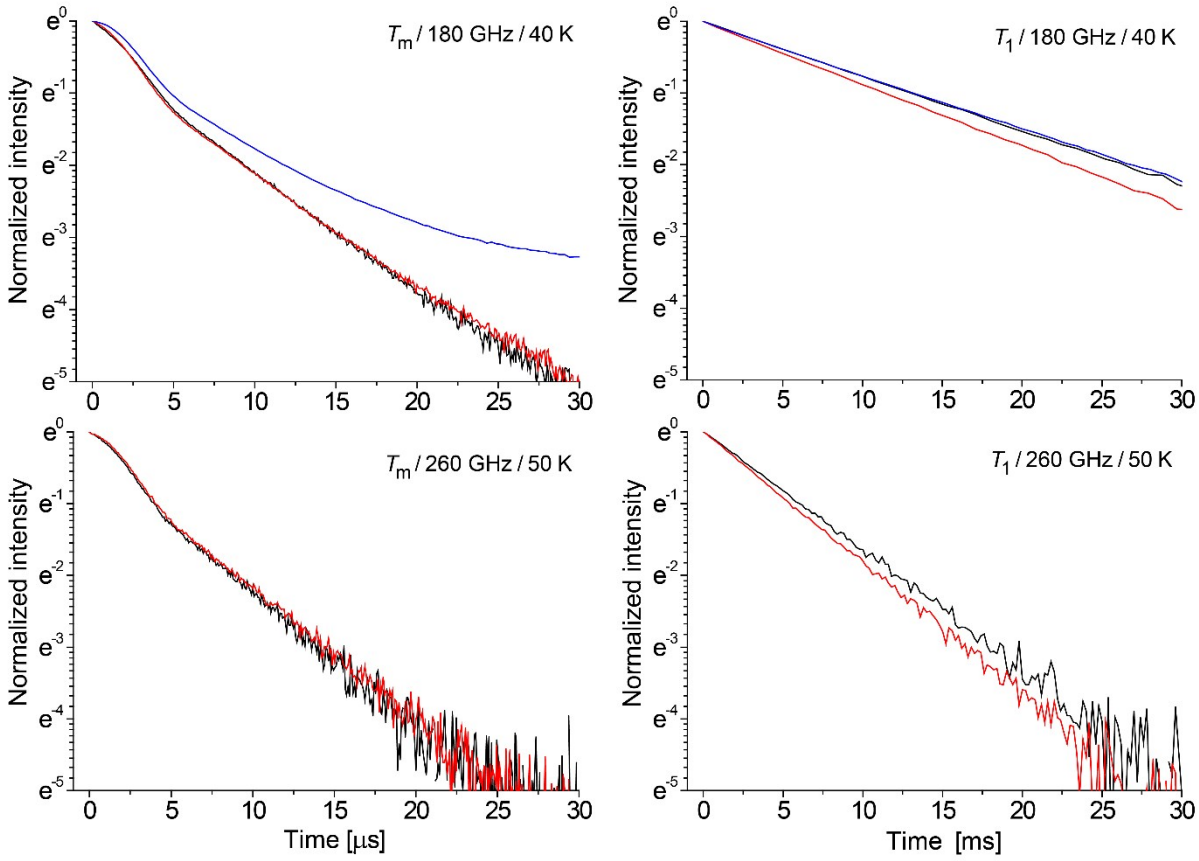

Figure S2. Electron spin relaxation time measurements for 10mer (black curve), 17mer DNA (red curve) and Finland trityl (blue curve only for 180 GHz) at a temperature of 40 K for 180 GHz and 50 K for 260 GHz measurements.

IV. Shaped broadband inversion pulse at 260 GHz

Amplitude and phase modulation of a sech/tanh pulse is defined by equation 1:

$$B_1(t) = B_{1max} \cdot sech(\beta t)$$

$$\varphi(t) = \int_0^t \omega(\tau)d\tau = \frac{BW_\infty}{\beta} \cdot ln[cosh(\beta t)],\ where\ \ \omega(t) = BW_\infty \cdot tanh(\beta t) \quad (1)$$

where t is defined in the time interval $[-t_p/2, t_p/2]$, t_p is the length of the pump pulse, B_{1max} is the maximum B_1 field, β is the truncation parameter and BW_∞ is the bandwidth of the pulse for an infinite value of βt (such that $tanh(\beta t) = 1$). The waveform for the in-phase and out of phase components of the pulse is given by equation 2:

$$S_{in-phase}(t) = B_1(t) \cdot cos(\varphi(t))$$
$$S_{out\ of\ phase}(t) = B_1(t) \cdot sin(\varphi(t)) \quad (2)$$

A more detailed description of shaped pulses is published elsewhere.[7,8] The parameters of the sech/tanh pulse used in this study are given in Table S2.

Table S2. Parameters of sech/tanh pulse

t_p, ns	400
β, MHz	3 ($1.2/t_p$)
BW_∞, MHz	39.8
B_{1max}, MHz	5

For the J-band PELDOR measurements a relatively small value for β (3 MHz which is equivalent to $1.2/t_p$) was used. This value was chosen as a compromise to obtain a relatively short pump pulse (length of 400 ns) with the very small maximal B_{1max} field strength (5 MHz) available in our spectrometer setup. Whereas longer pulse lengths would lead to a more smooth rectangular excitation profile in frequency space, they would smear out dipolar oscillations in the time trace.[7]

The sech/tanh pulse calculated with the parameters listed in Table S2 (also see equations 1 and 2) is shown in Figure S3.

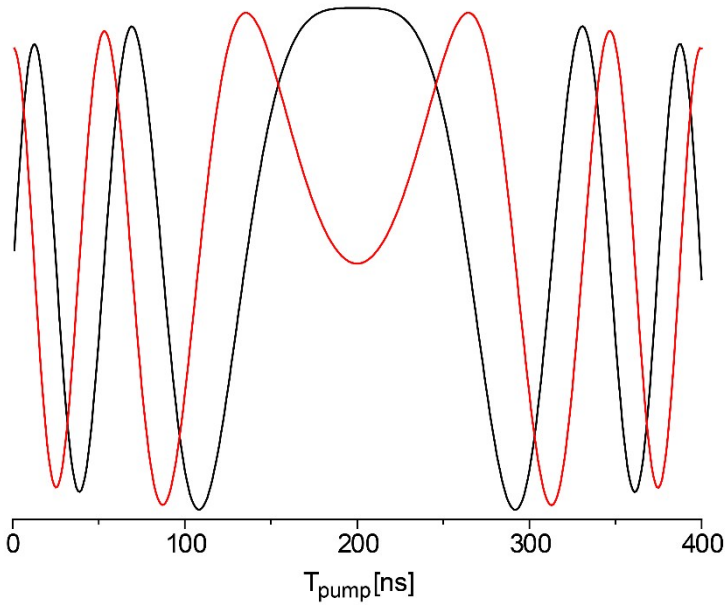

Figure S3. Shape of the sech/tanh pump pulse calculated with the parameters listed in Table S2 (calculations were performed using equations 1 and 2). Real and imaginary components are depicted in black and red, respectively.

PELDOR measurements were performed with a frequency offset between pump and probe pulses of Δν = -60 MHz. This offset was explicitly implemented in the calculation of the pulse shape, as given by equation 3:

$$S(t)_{complex}^{offset} = \left[B_1(t) \cdot cos(\varphi(t)) + i \cdot B_1(t) \cdot sin(\varphi(t))\right] \cdot e^{i \cdot 2\pi\Delta\nu t}$$
$$S_{in-phase}^{offset}(t) = real\left[S(t)_{complex}^{offset}\right] \quad (3)$$
$$S_{out\ of\ phase}^{offset}(t) = imag\left[S(t)_{complex}^{offset}\right]$$

In the J-band spectrometer the final 260 GHz pulses are created by three stages of frequency up-conversion. This results in 8 times multiplication of the initial AWG signal which is mixed with a local oscillator at Q-band. Therefore the original pulse shapes are loaded in the AWG with 8 times smaller phase and frequency steps with respect to the final wanted broadband pulse at J-band frequencies and are given by equation 4:

$$S(t)_{complex}^{offset/8} = \left[B_1(t) \cdot cos(\varphi(t)/8) + i \cdot B_1(t) \cdot sin(\varphi(t)/8)\right] \cdot e^{i \cdot 2\pi\Delta\nu t/8} \quad (4)$$

Thus, the pulse shape at J-band frequency depicted in Figure S3 is loaded into the spectrometer in a form shown in Figure S4.

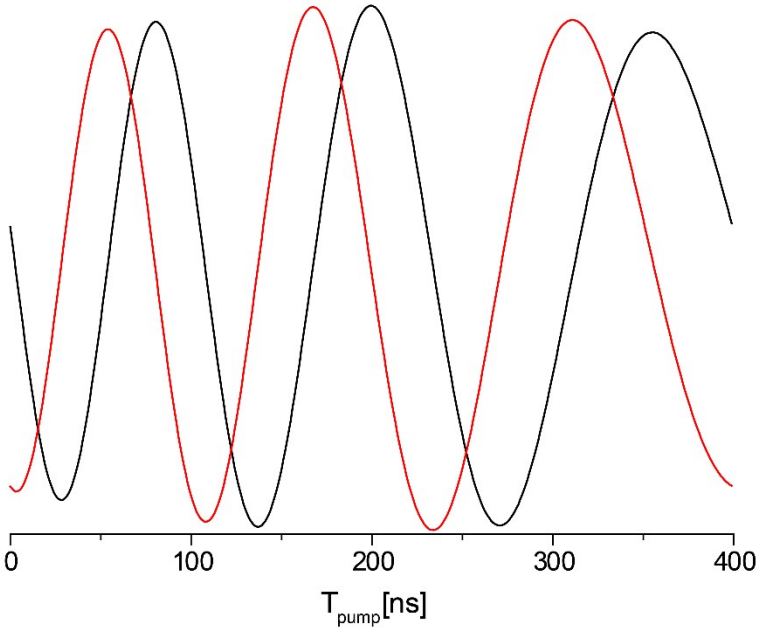

Figure S4. Calculated shape of the sech/tanh pump pulse, which is loaded into the J-band spectrometer. The shape corresponds to the one depicted in Figure S6, but with 8 times smaller phases and frequency offsets. Calculations were performed with the parameters listed in Table S2 and with an offset of -60 MHz with respect to a carrier frequency (at J-band frequencies) using equations 1 and 4. Real and imaginary components are depicted in black and red, respectively.

Accuracy in setting up the amplitudes and phases is an important issue for the performance of the broadband sech/tanh pulse. To check how precisely these parameters can be set with our J-band spectrometer, a Hahn echo signal was recorded with simultaneous sweep of the phase of both pulses ($\pi/2$ and π pulse), as shown in Figure S5.

As can be seen, the phase as well as the receiver signal intensity in both channels shows deviations from the ideal performance. Such deviations in phase of the pulse, as well as in amplitude arising from the non-linear up-conversion scheme and the resonator bandwidth, will influence the performance of the broadband shaped inversion pulses.

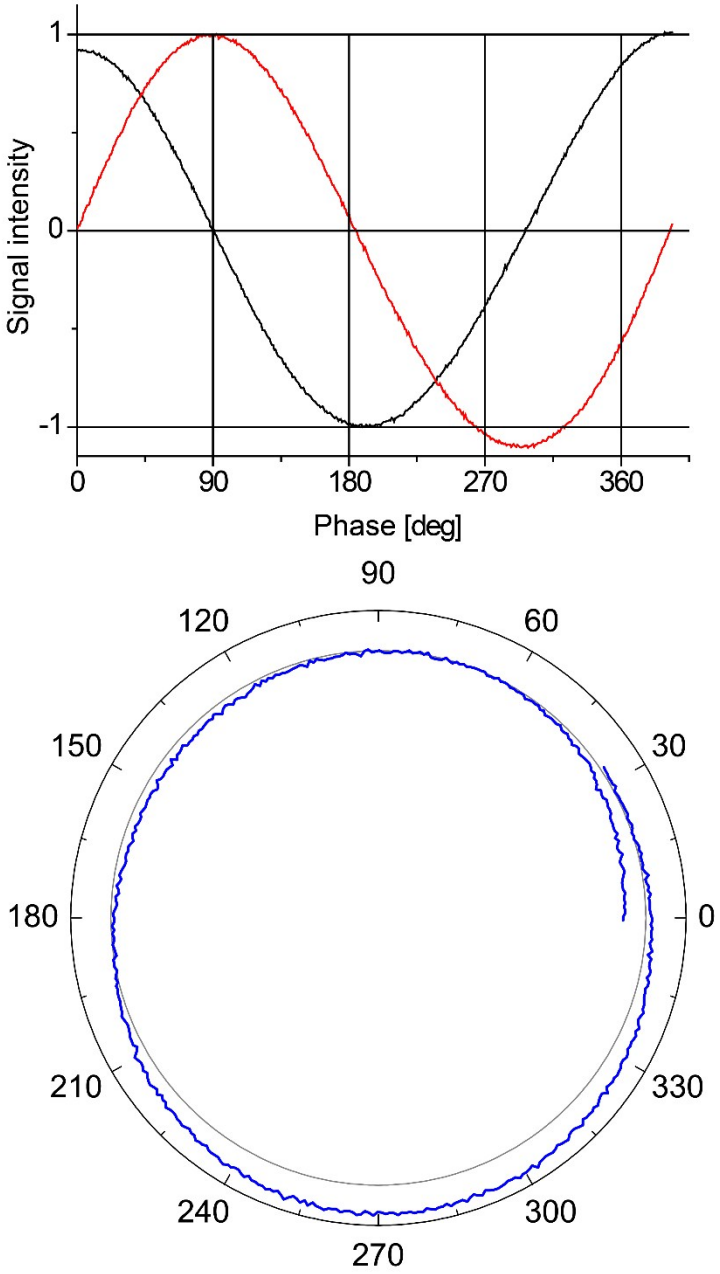

Figure S5. Experimentally measured integrated Hahn echo signal intensity as a function of the phase of the π/2 and π pulses on the10mer DNA sample. **Top:** real (black) and imaginary (red) components of the receiver signal. The signal intensities were normalized to the maximum of the real component. **Bottom:** The absolute value of the signal $\sqrt{Real^2 + Imag^2}$ as a function of the phase represented in polar coordinates.

Figure S6 compares the ideal pulse shape (calculated based on equations 1 and 3, using the parameters listed in Table S2 and an offset of -60 MHz with respect to the carrier frequency) with the experimentally measured pulse profile.

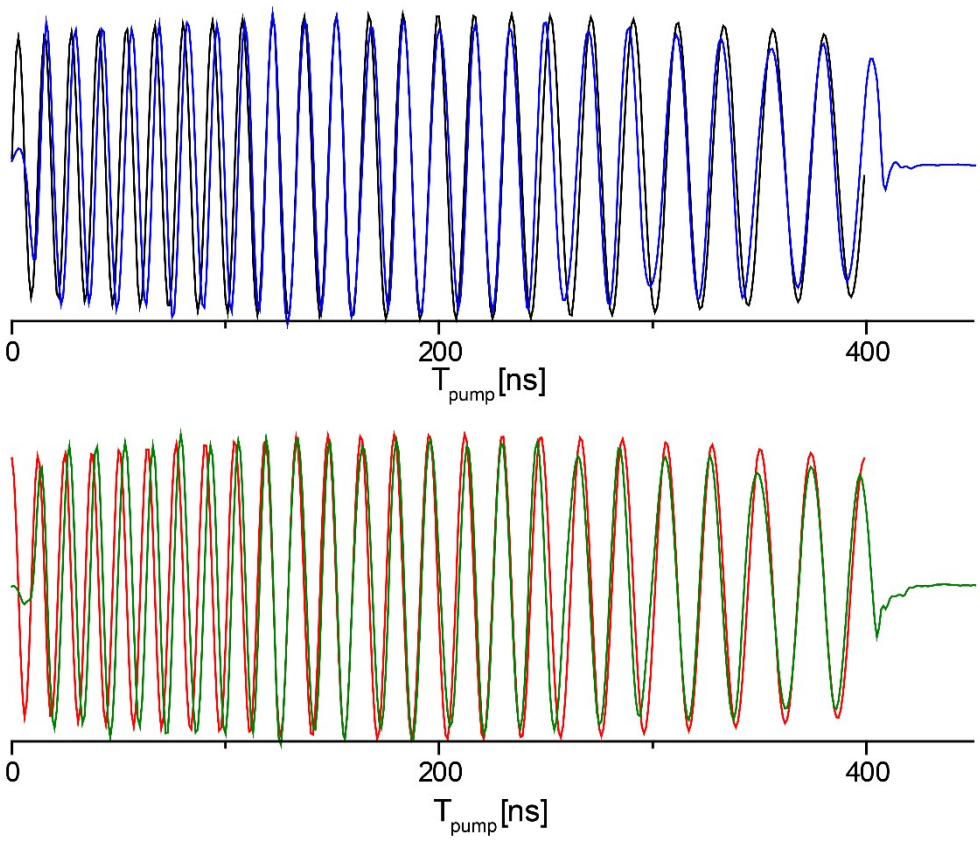

Figure S6. Comparison of the calculated and experimentally measured AWG pulse profiles. Upper traces: In-phase component of the receiver signal; Lower traces: 90° out-of-phase component of the receiver signal. The theoretically calculated shapes of the pulse listed in Table S2 with an offset frequency of -60 MHz with respect to the carrier frequency are depicted in black (real part) and red (imaginary part), whereas the experimentally measured pulse shape ones are depicted in blue (real) and green (imaginary). To detect the pulse shape directly by the SpecJet, the protection gate was removed and the microwave power attenuation was set to 28 dB (maximum attenuation). The video bandwidth of the receiver was 200 MHz and the quality factor of the resonator was about 1500 – 2000 resulting in a resonator bandwidth of about 175 MHz – 130 MHz.

The deviations between the shapes of the calculated and experimentally measured pulses are due to the above mentioned imperfections of phase and amplitude (in the transmitter as well as the receiver channel of the spectrometer) as well as the influence of the resonator as mentioned above. No attempts have been taken here to correct for these artefacts by compensating the input sequence of the AWG. In Figure S7 the inversion profiles calculated by a stepwise numerical application of the Bloch equation (for S=1/2 electron spins without dipolar coupling and with infinite long relaxation times) are compared. The integrated efficiency of a rectangular π π pulse with a length of 110 ns (black), of the theoretical broadband sech/tanh pulse with the parameters given in Table S2 (red) and the sech/tanh pulse observed by the SpecJet (blue) scales as 9.37/37.76/28.17. This leads to an enhanced inversion efficiency of the sech/tanh pulse of 4 (for the ideal sech/tanh pulse) and 3 (for the real sech/tanh pulse). This compares very well with the experimentally observed increase in modulation depth of a factor of 2.4 (10mer DNA) and 3.3 (17mer DNA) by application of the sech/tanh inversion pulse (see main text).

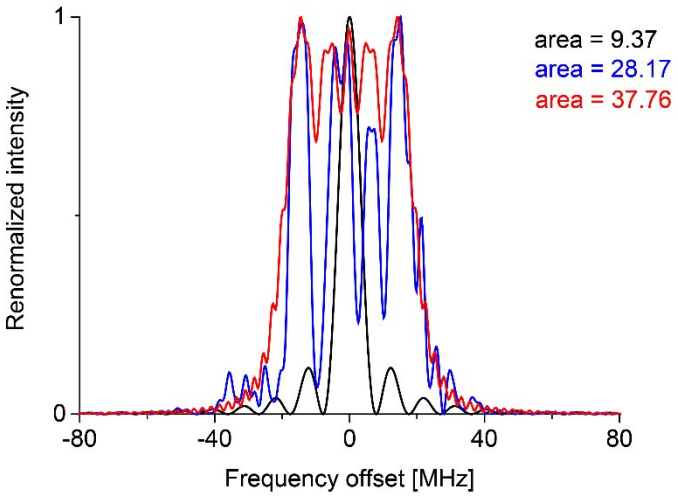

Figure S7. Comparison of the inversion profiles and efficiencies of a rectangular 110 ns inversion pulse (black), the theoretical calculated sech/tanh pulse with the parameters given in Table S2 (red) and the broadband pulse experimentally observed with the SpecJet (blue, see Figure S6). Calculations were performed using a home written code based on a numeric solution of the Bloch equations for a spin-1/2 without dipolar coupling and assuming very long relaxation times. The relative inversion efficiency of these pulses can be compared by integration over all offsets (area).

V. Experimental PELDOR data

The experimental PELDOR time traces obtained on the 10 and 17mer DNAs are depicted in Figure S8 for 180 GHz and in Figure S9 for 260 GHz frequencies with the corresponding exponential background functions.

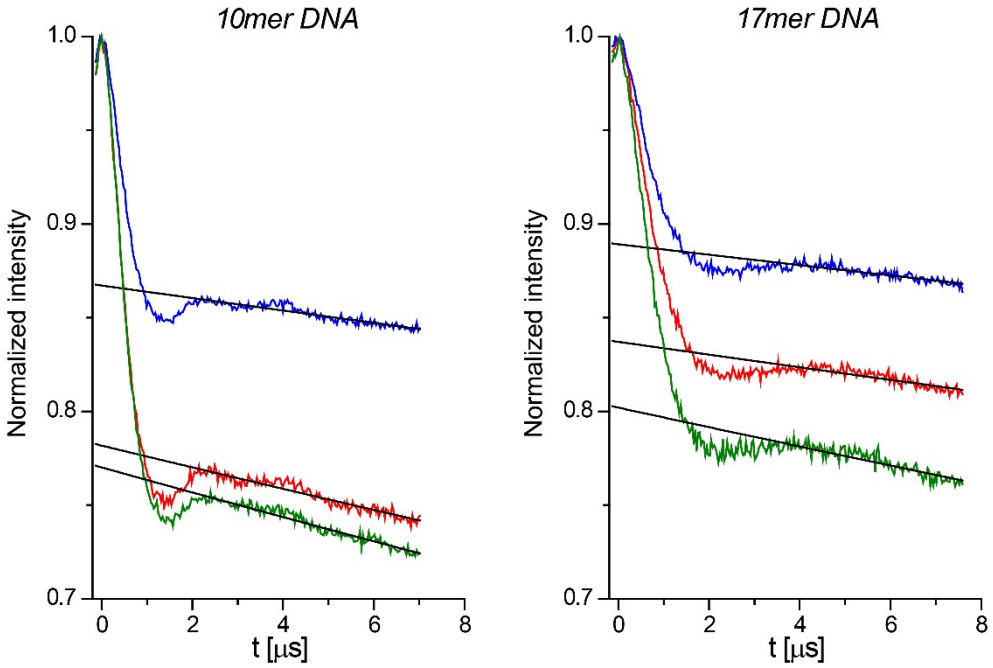

Figure S8. PELDOR time traces obtained at 180 GHz frequencies at a temperature of 40 K (colors correspond to the pump-probe positions given in Figure 1) and the corresponding exponential background functions (black curves).

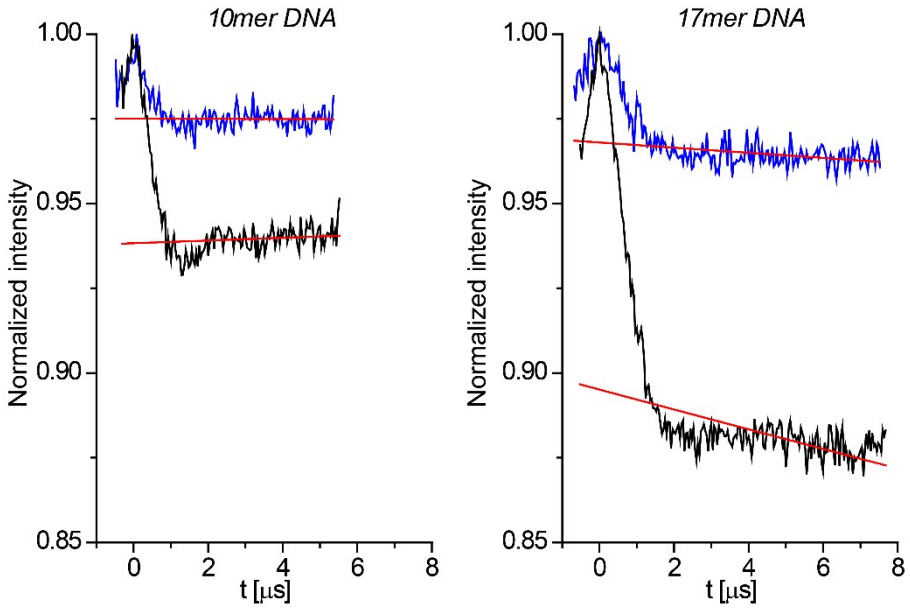

Figure S9. PELDOR time traces obtained at 260 GHz frequencies at a temperature of 50 K with rectangular (blue curves) and shaped (black curves) pump pulses and the corresponding exponential background functions (red curves).

VI. Sensitivity of PELDOR measurements

In order to assess the sensitivity per square root of time, the following algorithm was applied (see also the visual representation of the procedure given in Figure S10 and Figure S11 for 260 GHz and 180 GHz, respectively):

1) All the time traces were scaled to 100% modulation depth
2) Fit of the time trace by a 9th order polynomial function
3) Residuals between the experimental traces (black) and the fit (red) were calculated (blue)

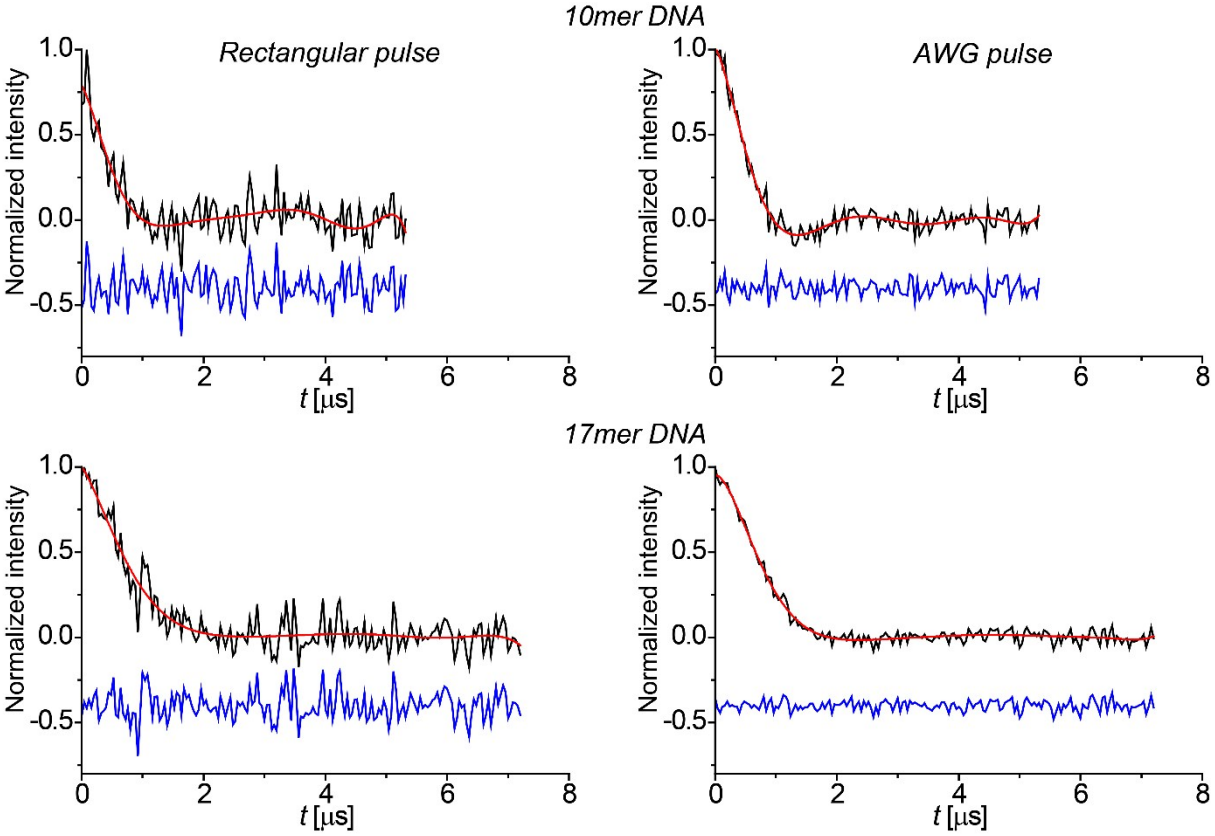

Figure S10. Procedure to calculate the signal-to-noise gain of the shaped inversion pulse. The modulation depth rescaled 260 GHz PELDOR time traces (black curves) with fits obtained by a 9th order polynomial function (red curves) and the remaining residuals (blue curve) are shown. For better visualization the residuals are vertically offset.

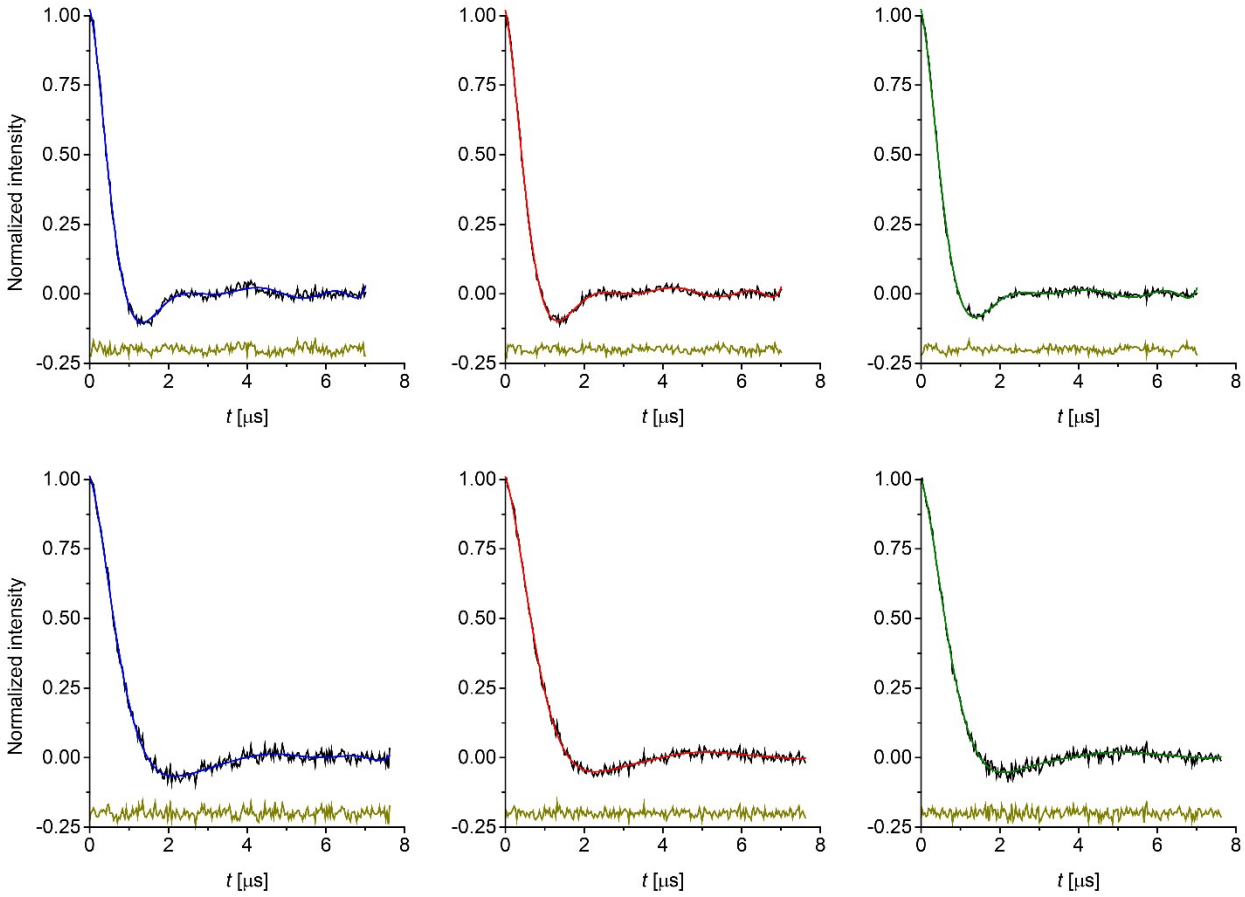

Figure S11. Procedure to calculate the sensitivity per square root of time for 180 GHz PELDOR measurements. The modulation depth rescaled 180 GHz PELDOR time traces (black curves) with fits obtained by a 9th order polynomial function (colour code is consistent with Figures 2 of the main text) and the remaining residuals (dark yellow curve) are shown. For better visualization the residuals are vertically offset. **Up:** 10mer DNA. **Bottom:** 17mer DNA.

The sensitivity per square root of the acquisition time is calculated as given by equation 5:

$$\sigma = \frac{\sqrt{\sum_{i=1}^{N} residual(i)^2}}{\sqrt{N}} \tag{5}$$

$$Sensitivity\ per\ square\ root\ of\ time = \frac{1}{\sigma\sqrt{t}}$$

where t is the acquisition time of the corresponding PELDOR time trace (calculated in hours). The results of the analysis are summarized in Table S3.

Table S3. Sensitivity per square root of time for PELDOR measurements at 180 GHz and 260 GHz and DQC experiments performed at 34 GHz

Frequency	Parameter/Time trace	Modulation depth		SNR/$\sqrt{t}$ [$\sqrt{h}$]	
		10mer DNA	17mer DNA	10mer DNA	17mer DNA
180 GHz	red	21.9%	16.4 %	63.2	37.1
	blue	13.2%	11.1%	45.1	38.3
	green	23.0%	20.0 %	47.3	30.3
260 GHz	Rectangular pulse	2.5%	3.5%	3.6	4.1
	Sech/tanh pulse	6.1%	11.5%	7.3	11.3
34 GHz	DQC	-	-	44.7	47

As can be seen, the sensitivities of G-band PELDOR and Q-band DQC are quite comparable. However, taking into account that the active sample volume for G-band is 200 nl and for Q-band it is 8 µl (the same DNA concentration was used), the former is about a factor of 40 more sensitive.

VII. Error estimates in distance distributions

Distance distributions with error estimates, performed with DeerAnalysis2013 toolbox, are given in Figures S12, S13 for 180 GHz and Figure S14 for 260 GHz PELDOR measurements.

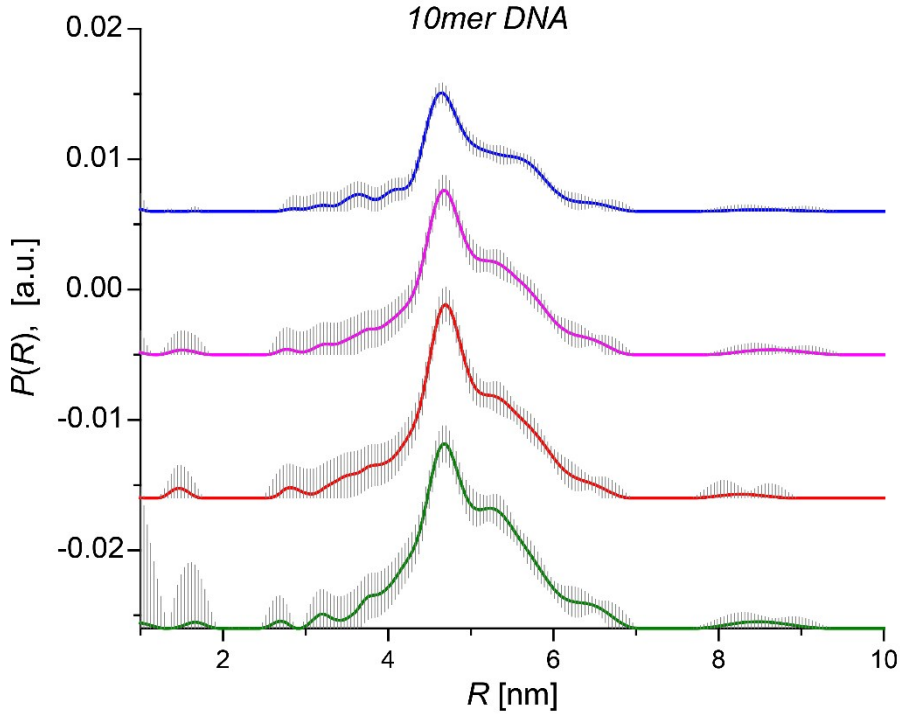

Figure S12. Distance distributions from 180 GHz PELDOR measurements on 10mer DNA (distance distributions are adapted from Figure 2 of the main text with remaining the colour code).

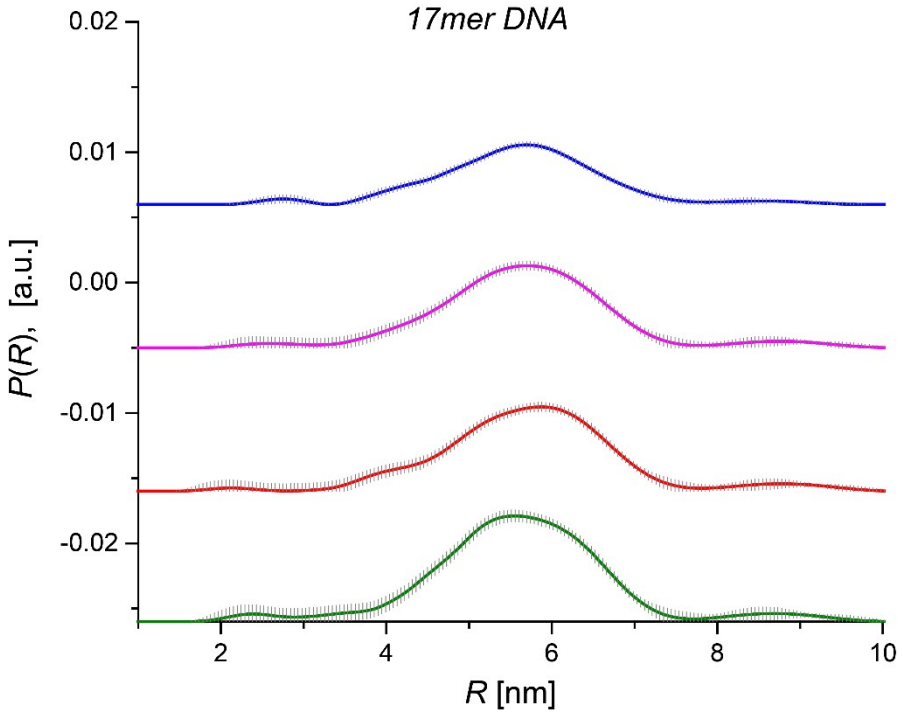

Figure S13. Distance distributions from 180 GHz PELDOR measurements on 17mer DNA (distance distributions are adapted from Figure 2 of the main text with remaining the colour code).

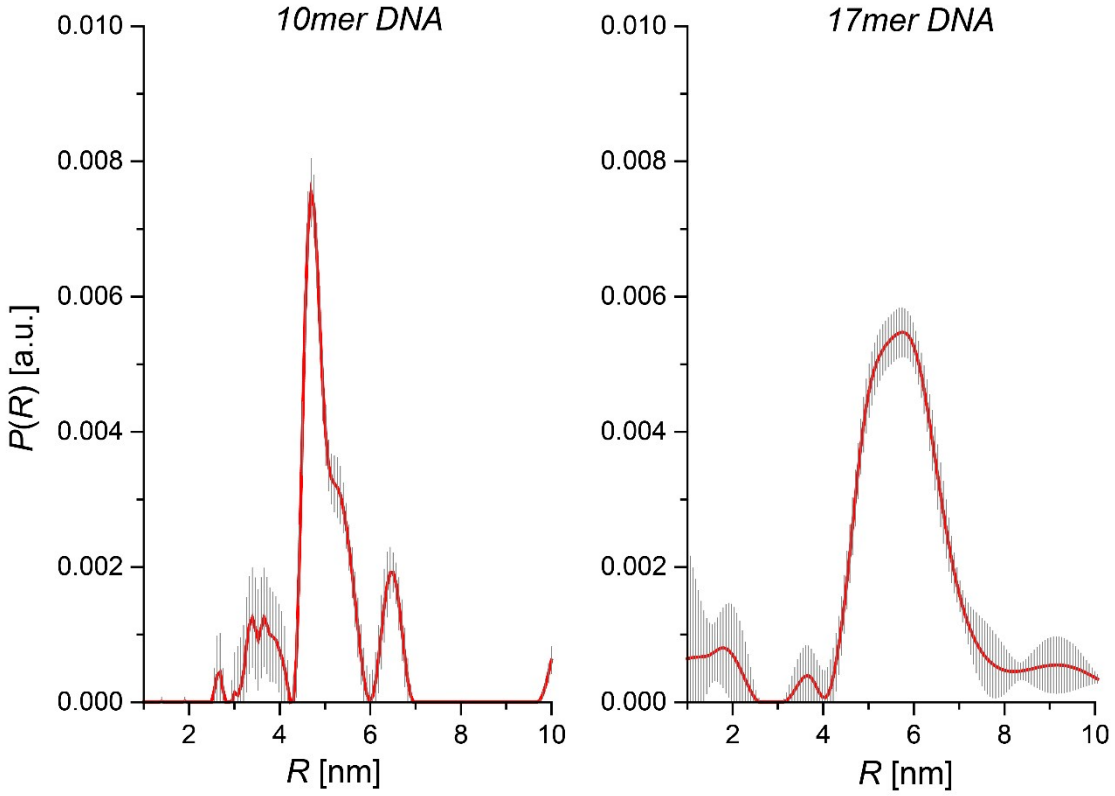

Figure S14. Distance distributions from 260 GHz PELDOR measurements with sech/tanh pump pulse (distance distributions are adapted from Figure 3 of the main text).

VIII. References

1. G. Yu. Shevelev, E. L. Gulyak, A. A. Lomzov, A. A. Kuzhelev, O. A. Krumkacheva, M. S. Kupryushkin, V. M. Tormyshev, M. V. Fedin, E. G. Bagryanskaya and D. V. Pyshnyi, *J. Phys. Chem. B*, 2018, **122**, 137.
2. M. Rohrer, O. Brügman, B. Kinzer and T. Prisner, *Appl. Magn. Reson*., 2001, **21**, 257.
3. V. Denysenkov, T. Prisner, J. Stubbe and M. Bennati, *Appl. Magn. Reson*., 2005, **29**, 375.
4. R. E.Martin, M. Pannier, F. Diederich, V. Gramlich, M. Hubrich and H. W. Spiess, *Angew. Chem., Int. Ed.*, 1998, **37**, 2833.
5. M. Pannier, S. Veit, A. Godt, G. Jeschke and H. W. Spiess, *J. Magn. Reson*., 2000, **142**, 331.
6. C. E. Tait and S. Stoll, *Phys. Chem. Chem. Phys.*, 2016, **18,** 18470.
7. P. E. Spindler, S. J. Glaser, T. E. Skinner and T. F. Prisner, *Angew. Chemie - Int. Ed*., 2013, **52**, 3425.
8. P. E. Spindler, P. Schöps, W. Kallies, S. J. Glaser and T. F. Prisner, *J. Magn. Reson.*, 2017, **280,** 30.